Physicochemical, Cytotoxic, and Dermal Release Features of a Novel Cationic Liposome Nanocarrier

Maura Carboni, Angela M. Falchi, Sandrina Lampis, Chiara Sinico, Maria L. Manca, Judith Schmidt, Yeshayahu Talmon, Sergio Murgia, and Maura Monduzzi*

A novel cationic liposome nanocarrier, having interesting performance in topical drug delivery, is here presented and evaluated for its features. Two penetration enhancers, namely monoolein and lauroylcholine chloride, are combined to rapidly formulate (15 min) a cationic liposome nanostructure endowed of excellent stability (>6 months) and skin penetration ability, along with low short-term cytotoxicity, as evaluated via the MTT test. Cytotoxicity tests and lipid droplet analysis give a strong indication that monoolein and lauroylcholine synergistically endanger long-term cells viability. The physicochemical features, investigated through SAXS, DLS, and cryo-TEM techniques, reveal that the nanostructure is retained after loading with diclofenac in its acid (hydrophobic) form. The drug release performances are studied using intact newborn pig skin. Analysis of the different skin strata proves that the drug mainly accumulates into the viable epidermis with almost no deposition into the derma. Indeed, the flux of the drug across the skin is exceptionally low, with only 1% release after 24 h. These results validate the use of this novel formulation for topical drug release when the delivery to the systemic circulation should be avoided.

1. Introduction

During the past decades advancement in bottom up/top down strategies have improved the ability in matter manipulation, thus favouring the proliferation of sophisticated nanocarriers able to deploy pharmaceutical cargos to specific tissue. Nowadays, along with traditional colloidal dispersions (i.e., micelles, microemulsions, liposomes, etc.),[1,2] the drug delivery systems arsenal also embraces polymer gels,[3,4] polyelectrolyte multilayer capsules,[5] as well as inorganic nanoparticles[6,7] and composite nanomaterials.[8]

In this context, lipid based self-assembled nanostructures always represent a powerful choice in virtue of their features and performances.[9–14] Moreover, given their intrinsic resemblance to biomembranes, they are greatly appreciated when studying drug/nanocarrier-cell interactions.[15–17] Liposomes, representing an emblematic example of this category, have been proposed since the early eighties as skin drug delivery systems.[18] Indeed, skin represents an appealing gateway for the delivery of drugs, especially when enteral administration cannot be pursued, or to achieve a better patient compliance.

Every system designed for the skin delivery should be able to favor the permeation of drugs to the deeper skin layers (the viable epidermis and eventually the vascularised derma). However, as in most cases traditional liposomes remain confined to the upper layer of the *stratum corneum* (SC), they were found inadequate for drug delivery through the skin.[19,20] Therefore, the original liposome nanostructures have been implemented by engineering new liposome nanocarriers variously termed Transferosomes®, ethosomes, or niosomes, depending on their peculiar features. Transferosomes® are liposomes that express high deformability because of the addition of an edge activator, a surfactant having a high radius of curvature that destabilizes the lipid bilayer.[21,22] Thanks to their elasticity they can squeeze between the corneocytes more easily, entering the deep skin layers. Ethosomes exploit the interdigitation effect of ethanol (which is part of their nanostructure) on lipid bilayers to enhance permeation.[23,24] Niosomes are vesicles composed of nonionic surfactants and having functions similar to liposomes.[25,26] It deserves noticing that, despite the huge number of papers published on this topic, the exact mechanisms that drive the penetration process still remain a matter of speculation.[27,28] However, from an empirical point of view, all these innovative nanocarriers have been found to increase both the

M. Carboni, Dr. S. Lampis, Dr. S. Murgia, Prof. M. Monduzzi
Department of Chemical and Geological Sciences
University of Cagliari
CNBS and CSGI, s.s. 554, bivio Sestu
09042 Monserrato (CA), Italy
E-mail: murgias@unica.it
Dr. A. M. Falchi
Department of Biomedical Sciences
University of Cagliari
s.s. 554, bivio Sestu, 09042 Monserrato (CA), Italy
Prof. C. Sinico, Dr. M. L. Manca
Department of Environmental and Life Science
University of Cagliari and CNBS
via Ospedale 72, 09100 Cagliari, Italy
Dr. J. Schmidt, Prof. Y. Talmon
Department of Chemical Engineering
Technion–Israel Institute of Technology
Haifa 3200, Israel

DOI: 10.1002/adhm.201200302

dermal and the transdermal release, often without being particularly selective in one sense or the other.[29]

Indeed, when delivering a drug through the skin, it is worth distinguishing between two possible, both desirable, results: the drug local accumulation into the skin (dermal release), or the permeation through the skin (transdermal release).[30] Plainly, the target of the drug will decide which of the two effects (accumulation or permeation) will be unwanted. For instance, a carrier developed for skin diseases such as autoimmune disorders (e.g., psoriasis), tumors, herpes, or erythema, should effectively cross the SC, and reach the deep skin layers, but, at the same time, should not be released into blood circulation, to avoid either waste of the drug (with the concomitant reduction of the therapeutic response) or side effects associated with systemic delivery (definitely, one of the main reason that underpins the dermal delivery strategy).[31] However, when targeting the drug delivery to the blood circulatory system high transdermal flux and low accumulation into the skin are required.

The present investigation is devoted to the evaluation of a novel liposome nanostructure proposed as a platform for the development of nanocarriers able to protect, transport, and release sensitive therapeutic agents.[32] Such a nanostructure is formulated by combining two penetration enhancers, namely monoolein and lauroylcholine chloride,[33,34] while diclofenac was added as a model hydrophobic drug. Here, this formulation was investigated for its physicochemical behaviour, short and long-term cytotoxicity, and dermal release properties.

2. Results and Discussion

2.1. Characterization of the Nanocarrier

A series of liposome samples with total monoolein (MO) concentration corresponding to around 4 wt% and increasing amount of lauroylcholine (LCh) were prepared by simply dispersing the components (MO and LCh) in water using an Ultra Turrax device as described in the Experimental section. Samples compositions are reported in **Table 1**.

The liposomes morphology was evaluated via transmission electron microscopy at cryogenic temperature (cryo-TEM). In **Figure 1**A,B we show micrographs representative of the discussed samples. As can be seen, though some larger bilamellar liposomes were also observed, these systems mainly consist of homogenously dispersed small unilamellar vesicles (SUVs).

Table 1. Liposome composition (wt%), mean diameter (nm ± SD), polydispersity index (PI), and zeta(ζ)-potential (mV ± SD).[a)]

Sample	MO/LCh/W	Mean diameter	PI	ζ-potential
LPS0.3	3.3/0.3/96.4	82 ± 23	0.325	57.3 ± 4.6
LPS0.4	3.2/0.4/96.4	82 ± 9	0.275	65.7 ± 1.1
LPS0.7	3.0/0.7/96.3	77 ± 26	0.292	71.0 ± 2.4
LPS1.3	2.5/1.3/96.2	87 ± 35	0.354	82.8 ± 0.5
LDH	3.3/0.3/96.4	202 ± 1	0.121	36.0 ± 0.8

[a)]LDH indicates the acid diclofenac loaded liposomes.

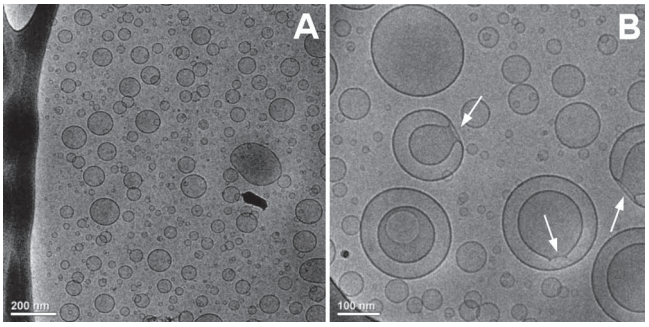

Figure 1. Cryo-TEM images of the sample LPS0.3 showing (A) unilamellar and (B) bilamellar liposomes. White arrows in B indicate interlamellar attachments (see the text).

Interestingly, some of the double walled liposomes show a defect (indicated by a white arrow), which is very common for this kind of nanostructure, the so-called interlamellar attachment (ILA). Such semi-toroidal bilayer attachments between flat bilayer sheets represent intermediates during the process of membrane fusion (as in this case) or phase transitions.[35] Results from dynamic light scattering (DLS, see Table 1) analysis confirm those previously discussed and collected via cryo-TEM. Accordingly, samples are composed by liposome having a mean diameter of about 80 nm and characterized by a relatively narrow size distribution, with a polydispersity index (PI) around 0.3.

The formation of MO-based SUVs is conditioned to LCh addition.[32] This short-chain surfactant intercalates between the MO palisade, decreasing the MO effective packing parameter (P_{eff}, defined as the ratio v/a_0l, where v is the volume of the surfactant tail, a is the cross-sectional area of the surfactant polar head, and l is the fully stretched length of the surfactant hydrophobic tail), and disturbing the regular arrangement of both the lipid tails and the polar heads. This allows for the bilayer folding toward the liposomal nanostructure. Consequently, the absence of correlation observed between the amount of LCh used for sample preparation and the size of the liposomes is quite surprising. This fact deserves some comments. The mechanisms that determine the stability, size and shape of the vesicles are complex and have been widely discussed.[36] Briefly, the bending of the lipid bilayer to form a vesicle imposes a strain on a symmetric bilayer, as the inner monolayer has a negative curvature, while the outer has a positive curvature. In many cases the magnitude of this curvature energy is thought to be significant enough to make the vesicles inherently unstable, and energy has to be added to allow bilayer folding. It follows that the liposome formation is favoured by soft bilayers, since less energy is required for the bending of the bilayer. Thus, it can be inferred that in these liposome formulations the inner structure of the dispersions is basically dictated by the energy input supplied through the Ultra Turrax device, rather than by the composition of the formulation. On the contrary, as reported in Table 1, liposomes exhibit a positive ζ-potential that, as expected, increases with LCh concentration. Collected values are in the range 57.3 - 82.8 mV. Since the ζ-potential reflects the net charge on the surface of the liposome, these values indicate the increased amount of the cationic surfactant entrapped within the MO

palisade, while varying samples composition and, at the same time, the good stability against aggregation and fusion of these colloidal suspensions. Sample stability was checked by visual (naked eye) inspection and measuring size distribution, polydispersity index, and ζ-potential during some months. Formulations have good long-term stability (when stored at room temperature), and appreciable variation of these parameters could not be detected even after six months.

Variable temperature SAXS experiments were also performed in the range of 25 - 55°C to evaluate thickness and stability of the lipid bilayer. Within the temperature range investigated, the bilayer thickness calculated with the Global Analysis Program (GAP, see the Experimental section) was found equal to 47 ± 1 Å. This value does not change significantly upon increasing the temperature and/or the LCh amount, thus highlighting once again the high stability of these formulations. It should be remarked that these fully hydrated bilayers are thicker with respect to that measured in the lamellar phases of the MO/water binary system (water content around 15%) for which a structure parameter of 42 Å was assessed.[37]

2.2. Cytotoxicity Assays

Given the potential application of these liposome formulations as drug carriers, their toxicity against mouse 3T3 fibroblasts was evaluated in vitro at different incubation time (2, 4, 24, 48 h) according to the MTT assay (which measures levels of metabolically active mitochondrial dehydrogenase enzymes). As shown in **Figure 2**, compared to untreated control cells sample LPS0.3 did not show a significant cytotoxic activity in the first 4 h of incubation time. Differently, a statistically significant cytotoxic effect could be observed with LPS1.3. In this case the treatment caused more than 50% of cell death. At long-term exposure (24, 48 h), both liposome formulations induced massive cell death (more than 80% cell killing).

Cytotoxicity experiments were supported by fluorescence microscopy observations of 3T3 cells that had been previously treated with the liposomes under the same conditions and, after liposome wash-out, were co-loaded with Nile Red and Hoechst probes to identify lipid droplets and nuclear morphology, respectively. Lipid droplets are dynamic organelles mainly involved in fat storage (essentially neutral lipids as triacylglycerols and cholesteryl esters) used for lipid metabolism and the synthesis of membrane lipids. Upon short time exposure (2, 4 h) to LPS0.3 liposomes, cells did not show any changes either in the morphology or in the intracellular membrane compartments, while chromatin condensation was not detected. Conversely, enhanced lipid droplet formation was observed, suggesting that cells were able to produce and accumulate triacylglycerols from MO-based liposomes (**Figure 3**B). In contrast, treatment of 3T3 cells with LPS1.3

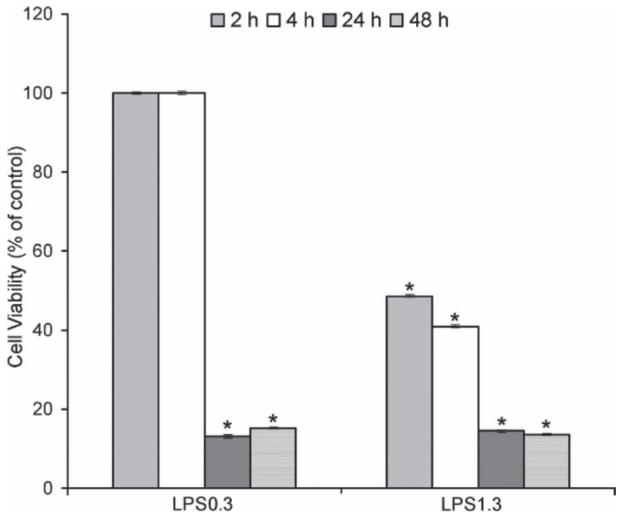

Figure 2. Results of MTT assay of the 3T3 cells exposed to the liposome formulations (1:200, 2.5 µL of liposome formulation in 500 µL of medium). 3T3 fibroblasts were incubated with liposomes formulation for 2, 4, 24, 48 h. Cell viability was determined by using the MTT reagent. The percent of treated cells was normalized to the untreated control cells. Error bars indicate the standard deviation of three different experiments with three duplicates per experiments. Statistically significant differences are indicated by $* p < 0.001$ vs. untreated cells by *t*-test.

formulation led to the appearance of proapoptotic cells with condensed cell nuclei, and altered intracellular lipid distribution. The red fluorescence of polar lipids in the cytoplasmic membranes appeared very strong, and the green fluorescence of lipid droplets was less visible and intense compared to control cells (Figure 3C). At long exposures (24, 48 h) both

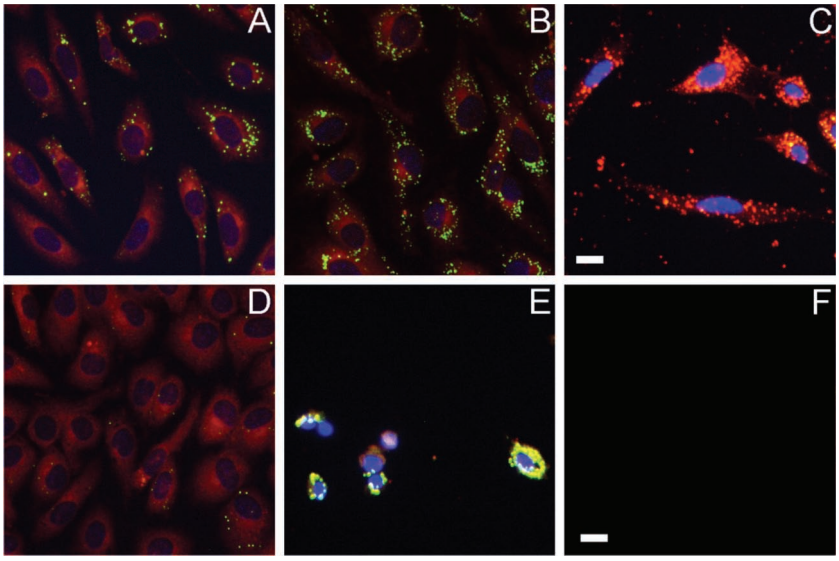

Figure 3. Representative composite color images of the 3T3 cells exposed to the liposome formulations. Membranes (red) and lipid droplets (green) were stained with Nile Red (colocalization in yellow), nuclei (blue) with Hoechst 33258. A, B, C: short-time treatments (2, 4 h). (A) control cells, (B) cells treated with LPS0.3 liposomes, (C) cells treated with LPS1.3 liposomes. D, E, F: long-time treatments (24, 48 h). (D) control cells, (E) cells treated with LPS0.3 liposomes, (F) cells treated with LPS1.3 liposomes. Scale bars = 20 µm.

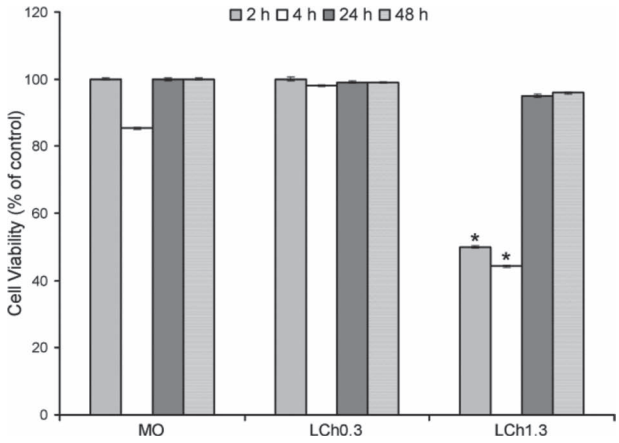

Figure 4. Results of MTT assay of the 3T3 cells exposed to MO and LCh solutions. 3T3 fibroblasts were incubated with monoolein (430 µM) and LCh solutions (47 and 202 µM) for 2, 4, 24, 48 h. Cell viability was determined by using the MTT reagent. The percent of treated cells was normalized to the untreated control cells. Error bars indicate the standard deviation of three different experiments with three duplicates per experiments. Statistically significant differences are indicated by $* p < 0.001$ vs. untreated cells by *t*-test.

liposome formulations induced massive cell death as shown by detection of rare apoptotic cells with chromatin condensation (Figure 3E, F).

Subsequently, the cytotoxicity of MO and LCh solutions were examined through the MTT assay. When exposed to MO or LCh0.3 alone, either at short or at long incubation time, the treatment did not cause cell death (**Figure 4**). On the contrary, more than 50% of cells treated with LCh1.3 formulation showed significant toxicity at short incubation time compared to un-treated control cells, MO and LCh0.3-treated cells. Remarkably, at longer incubation periods cells regained their normal proliferation capacity.

Figure 5 shows that MO and LCh-treated cells display extensive deposits of lipid droplets, which increase with exposure time. After short treatment with sample LCh1.3, the living cells (50% viability) showed chromatin condensation with intense red fluorescence of the cytoplasmic membranes (see Figure 5C). However, at longer incubation periods, cells regained their normal proliferation capacity as shown by normal chromatin condensation and cell culture confluence (see Figure 5F).

2.3. Lipid Droplet Evaluation

Lipid droplet formation is usually induced by long-chain unsatured fatty acid such as oleic acid.[38] Administration of exogenous unsatured fatty acids, especially oleic acid (one of the most frequently used unsatured fatty acid penetration enhancer), has been reported to increase membrane permeability even if their mechanism of action has not been completely elucidated.[39] After their internalization, free fatty acids are converted to fatty acyl-CoA, which can be either oxidized in mitochondria, or utilized in the endoplasmic reticulum as substrate for the synthesis of phospholipids, cholesterol esters and triacylglycerols.[40] Fluorescence-based detection of lipid droplets is commonly achieved in live cells with the green emission of Nile Red. To examine the possible role of liposome formulations in the lipid droplet formation, treatments were applied to semi-confluent monolayer of 3T3 cells, which contained few lipid droplets. Indeed, lipid droplets of 3T3 fibroblasts are present in high number in proliferating cells, but this number decreases in semi-confluent cells, and strongly diminishes when cells arrive at confluency and stop proliferation due to contact inhibition.[41]

After liposome treatment, the lipid droplet formation was examined with green-emission of Nile Red in comparison to untreated cells (as a control), oleic acid-treated cells (as a positive control) and monoolein-treated cells. Experiments were performed only at short-term incubation (2, 4 h, see **Figure 6**), because long-term exposure induced massive cell death. Compared to MO-treated cells, statistically significant increased production of lipid droplets was detected with LPS1.3 formulation treatment, whereas no differences were detected with LPS0.3 treatment. This result confirms the strong internalization ability of LCh.

OA and MO-treated cells were able to proliferate normally, produce and accumulate neutral lipids in form of lipid droplets also at longer exposition time, where, however, lipid droplets appeared aggregated into large clusters, thus preventing the quantification of the lipid droplet as illustrated in **Figure 7**, where long-term experiments are reported.

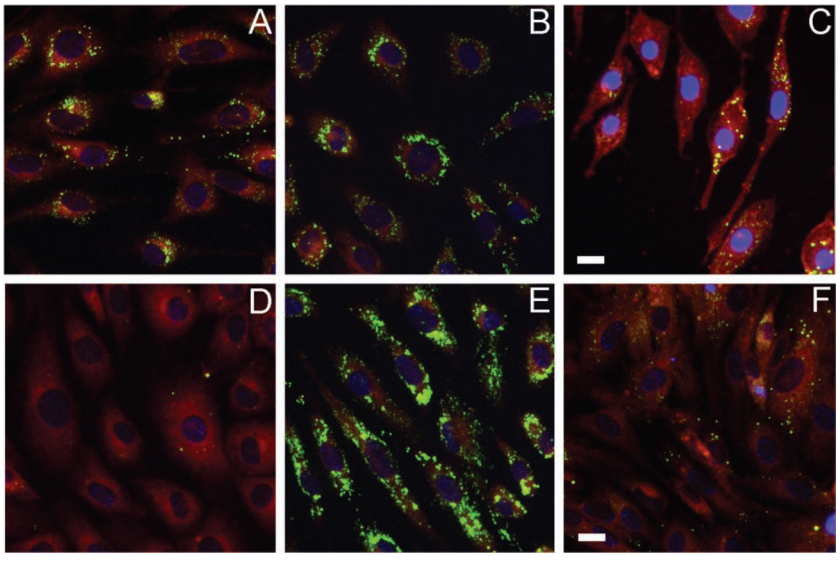

Figure 5. Representative composite color images of 3T3 cells exposed to the MO and LCh solutions. Membranes (red) and lipid droplets (green) were stained with Nile Red (colocalization in yellow), nuclei (blue) with Hoechst 33258. A, B, C: short-time treatments (2, 4 h). (A) control cells, (B) cells treated with MO, (C) cells treated with LCh1.3 solution. D, E, F: long-time treatments (24, 48 h). (D) control cells, (E) cells treated with MO, (F) cells treated with LCh1.3 solution. Scale bars = 20 µm.

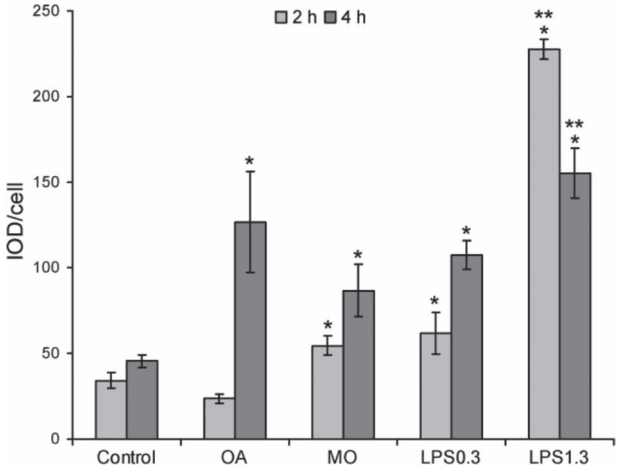

Figure 6. IOD (Integrated Optical Density) per cell related to lipid droplets formation in 3T3 cells exposed to the oleic acid (OA), monoolein (MO) and liposome (LPS) formulations. Quantification of lipid droplets in 3T3 fibroblasts incubated with OA (100 μM), MO (430 μM) and liposomes was performed with Image Pro Plus. Error bars indicate the standard deviation of at least two independent experiments. Statistically significant differences are indicated by * $p < 0.001$ versus untreated control cells and by ** $p < 0.001$ versus monoolein-treated cells by *t*-test.

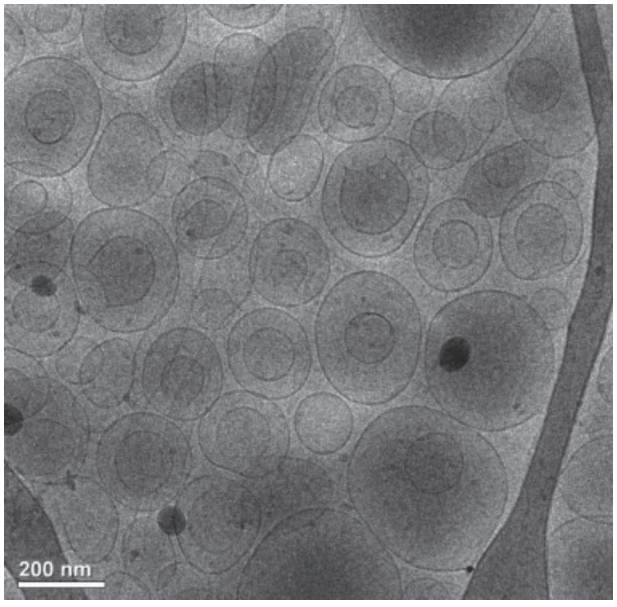

Figure 8. Cryo-TEM image of the sample LPS0.3 loaded with 0.97 mg/mL of acid diclofenac (LDH formulation).

2.4. Characterization of the Drug Loaded Nanocarrier

To check the ability of these innovative formulations in hosting molecules of pharmaceutical interest, diclofenac (DCFH) was added in its acid form (LDH, drug loaded liposome formulation). On the basis of the cytotoxicity tests the formulation with the lowest content of cationic surfactant (LPS0.3) was chosen. This formulation can nominally host 0.1 wt% of DCFH.

Acid diclofenac may interact with the lipid bilayer leading to modifications in the membrane properties. Therefore, the influence of drug encapsulation on the liposome nanostructure was investigated. Measurements on liposomes loaded with drug were performed after separation of non-encapsulated active molecule.

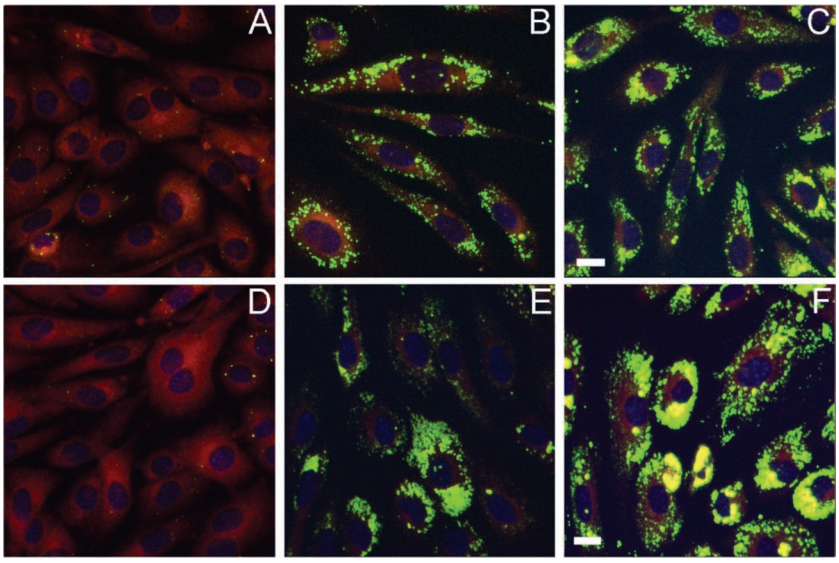

Figure 7. Representative composite color images of 3T3 cells exposed to the oleic acid and monoolein at 24 and 48 h of incubation time. Membranes (red) and lipid droplets (green) were stained with Nile Red (colocalization in yellow), nuclei (blue) with Hoechst 33258. A, B, C: 24 h treatment. (A) control cells, (B) cells treated with oleic acid, (C) cells treated with monoolein. D, E, F: 48 h treatment. (D) control cells, (E) cells treated with oleic acid, (F) cells treated with monoolein. Scale bars = 20 μm.

Before discussing the role of DCFH in the morphological changes of the liposomes, it deserves noticing that diclofenac has a solvophobic behavior that depends on pH. Actually, it was found that this molecule predominantly exists in its acid (hydrophobic) form at pH 3.0, while at pH 7.4 this molecule is almost completely present in its ionized (hydrophilic) form.[42] Since in LPS0.3 and LDH formulations pH 4.5 and 3.0 were respectively measured, it can be safely assumed that all the loaded diclofenac is in its hydrophobic form.

The cryo-TEM analysis revealed that the vesicular structure was maintained after the addition of low levels of DCFH, but liposomes increase in size, while the morphology is altered to some extent (see **Figure 8**). Indeed, along with approximately spherical liposomes some elongated elliptical liposomes are also observed in LDH formulation. DLS measurements confirm the huge increase of liposomes size, with respect to empty liposomes formulations, with a mean diameter varying from about 80 to 200 nm (see Table 1). In addition, bilamellar nanostructures are

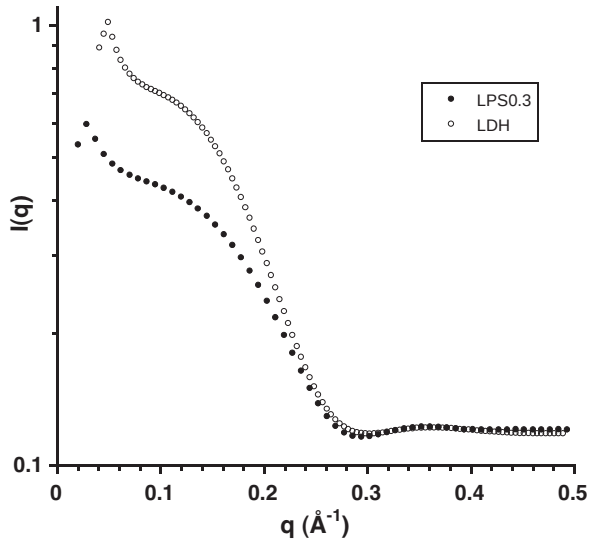

Figure 9. SAXS patterns of empty (LPS0.3) and drug loaded (LDH) liposomes.

present in higher numbers, and they appear slightly deformed compared to liposomes without the drug.

Taken as a whole, these results strongly suggest that DCFH, intercalating within the bilayer, modifies the lamellar bending. The effect of the encapsulation of the drug can be interpreted as follows.

Preferred location of DCFH within the bilayer leads to an increment of the hydrophobic tails volume and, in turn, to a greater value of the effective packing parameter. It is worth to recall here that a reduction of MO P_{eff} was called into play to justify the liposome formation (see above). Hence, the DCFH molecule operates against the effect of the LCh surfactant (causing a more rigid bilayer) and partially re-establishes the flatness of the original MO bilayer.

Concerning the measured ζ-potential, it is interesting to point out that the addition of only 0.1 wt% (0.97 mg mL^{-1}) of DCFH decreases the vesicle charge of about 20 mV. Indeed, the ζ-potential shift due to the DCFH loading was expected to a lesser extent because of its inclusion within the lipid palisade.

SAXS analysis through GAP of the drug-loaded system showed an almost unchanged d_B value of the liposomes bilayer in the LDH formulation (46 Å) with respect to that measured in the blank system (47 Å). **Figure 9** shows the SAXS patterns obtained from the LPS0.3 and LDH formulations. Although in the LDH formulation cryo-TEM analysis indicated a strong presence of bilamellar vesicles, the contribution of these structures does not emerge in the SAXS pattern. Therefore, it can be properly fitted with pure diffusing scattering model, the same used for unilamellar vesicles (see the Experimental Section). The best fit parameter from the GAP modeling of the SAXS patterns are given in **Table 2**. For all the formulations examined, such analysis gives for the z_H parameters (which essentially represents the length of the MO hydrocarbon chain, see **Scheme 1**) a value very close to that reported in literature for MO-based nanostructures (17 Å).

Table 2. Best fit parameters (z_H and σ_H are reported in Å) for the SAXS patterns obtained through GAP modeling at 25 and 55 °C.

Sample	25 °C		55 °C	
	z_H	σ_H	z_H	σ_H
LPS0.3	15.6 ± 0.3	4.1 ± 0.3	15.0 ± 0.4	3.7 ± 0.5
LDH	15.0 ± 0.1	3.9 ± 0.2	14.9 ± 0.2	3.9 ± 0.4

2.5. Ex Vivo Skin Penetration and Permeation Tests

Liposomes were able to encapsulate large amount of DCFH (E% ~ 51%). To evaluate the capability of this carrier to enhance the dermal and transdermal delivery of DCFH, a permeation study by using the Franz cell apparatus and newborn pig skin was carried out through the whole skin and in non occlusive condition for 24 h. In **Figure 10** the amount of permeated DCFH per area is plotted against time, and is compared with a gel formulation having the same drug concentration. Examination of the permeation graphs suggests that the systems under consideration reached steady-state conditions, but after different lag times. DCFH showed a shorter lag time (2 h) when incorporated in gel formulation, while in liposomal formulation, because of the very low flux obtained, it was not possible to calculate a lag time value from the curve. The mean amount of the drug permeated after 24 h experiment from the gel was 15.81 μg cm^{-2}, while 0.72 μg cm^{-2} DCFH was delivered by the liposomes. The latter value appears extremely low. It means that after 24 h only 1% of the drug is released through the skin. The Local Accumulation Efficiency (LAC) values, representing the ratio of diclofenac accumulated into the whole skin versus that permeated through the skin, was also calculated. The lowest

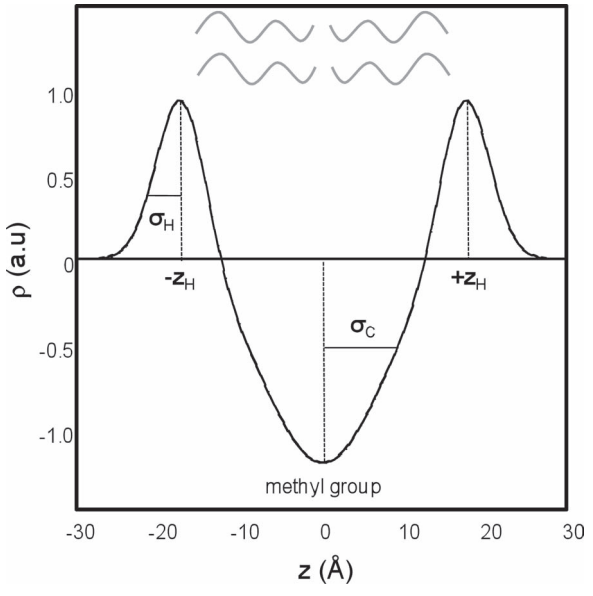

Scheme 1. Electron density profile (ρ) as a function of the distance from the bilayer centre, modelled by a summation of three Gaussians.

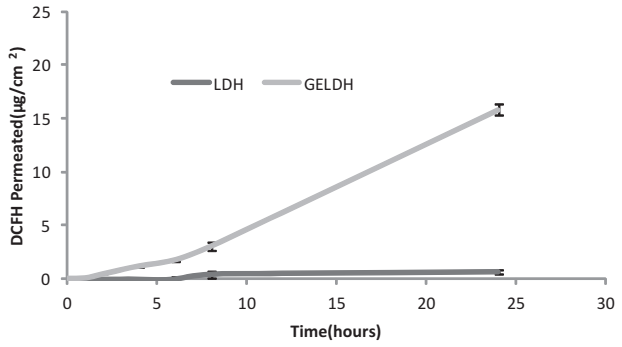

Figure 10. Ex vivo permeation of DCFH through newborn pig skin from liposomes and gel formulation (control). Each value is the mean ± standard deviation of six experimental determinations.

LAC value was obtained with DCFH loaded gel (0.23), while an anomalously high value (25.31) was found when the DCFH loaded liposome formulation was used.

In **Figure 11** the amounts of drug accumulated into the different skin layers are reported. Remarkably, DCFH accumulation was enhanced when the liposomal formulation was used. In particular, the presence of DCFH was predominantly recorded into the viable epidermis, while deposition into the dermis was only 0.02%. When the gel formulation containing the same amounts of the drug is used, DCFH mainly accumulated into the SC (only 0.04% of DCFH was found in the dermis). These data prove that LDH formulation was able to induce drug accumulation into the skin strata with a very poor transdermal delivery.

Liposome flexibility is often called into play to explain enhanced dermal and transdermal delivery, therefore a measurement of the liposome bilayer deformability was carried out by the extrusion method. Since LDH dispersion was not able to pass through filters of 50 nm pores size, these experiments definitely certify the low deformability of this kind of vesicles.

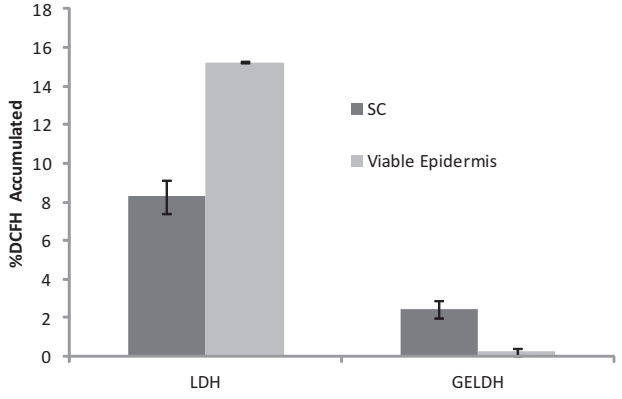

Figure 11. Cumulative amount of DCFH retained into newborn pig skin layers after 24 h non-occlusive treatment with liposomes and gel formulation (control). Each value is the mean ± standard deviation of six experimental determinations.

3. Conclusions

We tested a novel cationic nanocarrier for its physicochemical, cytotoxicity, and drug release features.

In spite of the very fast method of preparation (about 15 min) and the absence of any method for the improvement of particle size, Cryo-TEM, SAXS, and DLS experiments highlighted that monoolein and lauroylcholine self-aggregate to form a fairly low polydispersed, robust liposome nanostructure.

Microscopy investigation of living cells and cell viability assays demonstrated that, at short exposure time and low LCh content, liposomes are not toxic. Differently, at long exposure time and/or for high LCh content, they cause extensive cells death. Lipid droplets accumulation also shown that LCh favors internalization. In addition, it was found that at high concentrations and for a short-term treatment, LCh provoked a statistically significant toxic effect that cells were able to repair at longer incubation time, while MO did not affect cells viability at all. On the ground of these results, it can be inferred that the synergistic effects of MO and LCh, regarded as membrane penetration enhancers, is accountable for the observed cytotoxicity of liposome formulations. Another aspect that should be considered is the local concentration of the two penetration components that, with respect to the MO or LCh solutions, is much higher when the cells are exposed to the liposomes formulations, thus provoking greater damages to the cell plasma membrane and intercellular membranes.

The efficacy of a skin penetration enhancer depends on composite physicochemical factors, as well as whether the enhancer is used alone or in combination.[43] And the strength of penetration is usually directly proportional to skin irritation (i.e., cytotoxicity).[44] Indeed, the action of an effective penetration enhancer cannot be limited to the skin superficial layers. Rather, diffusing through the SC it reaches the viable epidermis (exactly the scope to which the nanocarrier is designed for). There, the same factors that improve the drug penetration may alter the keratinocyte membranes, thus provoking cytotoxicity. Therefore, the development of an effective drug delivery system able to enhance skin penetration without altering the normal cell viability can be regarded as a real challenge.

The skin penetration mechanism is highly debated, and different hypothesis have been proposed to explain the superior liposome efficiency in dermal and transdermal drug release. These include intact vesicles skin penetration (ultraflexible liposome), vesicle adsorption to and/or fusion with the SC (increased partitioning of the drug into the skin), and structural loosening of the intercellular lipid matrix due to the penetration enhancing action of the vesicle components.[27] Deformability test and release data ruled out that the cationic liposomes discussed here may cross the skin intact. Definitely, given their low flexibility, it is difficult to believe they can pass through the (one order of magnitude smaller) skin intercellular path. In addition, this fact may explain the negligible amount of drug found in the receptor compartment of the Franz cell. Once out of the liposome nanostructure the hydrophobic DCFH remains embedded into the skin rather than diffuse into the physiological solution. Conversely, taking into account the particular composition of the proposed nanocarrier, it is very likely that both MO and LCh alter the intercellular lipid matrix, facilitating

drug penetration through the SC and accumulation into the viable epidermis.

On such basis, this novel formulation can be regarded as an useful nanocarrier for topical drug release, when the systemic delivery ought to be kept to the minimum.

4. Experimental Section

Materials: Monoolein (MO, 1-monooleoylglycerol, RYLO MG 90-glycerol monooleate; 98.1 wt% monoglyceride) was kindly provided by Danisco Ingredients, Brabrand, Denmark. Lauroylcholine chloride (LCh) was from TCI Europe. Distilled water, passed through a Milli-Q water purification system (Millipore), was used to prepare the samples. Diclofenac free acid (DCFH) was obtained by acidic precipitation from a solution of sodium diclofenac purchased from Sigma–Aldrich (Milan, Italy). All substances were used without further purification. All concentrations are given in% (wt/wt).

Liposome Preparation: Liposomes, empty or loaded with DCFH (0.97 mg mL^{-1}), are obtained by dispersing weighed amount of MO in aqueous solutions containing LCh using an Ultra-Turrax T10 (IKA) device, equipped with a S10N-5G dispersing tool working at 30000 rpm for 10 minutes. Vesicles characterization was performed as a function of cationic surfactant content, the total dispersed phase (MO + LCh) was between 3.5–3.8 wt%. The sample volume was usually 3 mL. To obtain drug-loaded liposomes, DCFH was dissolved in the melted monoolein before Ultra-Turrax dispersion. All the samples were analyzed at least 48 h after their preparation. Vesicles loaded with drug were analyzed after separation of non encapsulated drug.

Cryogenic-Transmission Electron Microscopy (cryo-TEM): Vitrified specimens were prepared in a controlled environment vitrification system (CEVS), at 25 °C and 100% relative humidity. A drop of the sample was placed on a perforated carbon film-coated copper grid, blotted with filter paper, and plunged into liquid ethane at its freezing point. The vitrified specimens were transferred to an Oxford CT-3500 cooling holder, and observed at 120 kV acceleration voltage in an FEI T12 transmission electron microscope at about –180 °C in the low-dose imaging mode to minimize electron-beam radiation-damage. Images were digitally recorded with a Gatan US1000 high-resolution CCD camera.

Dynamic Light Scattering (DLS) and Zeta (ζ)-Potential Experiments: Particle size and ζ-potential determinations of the vesicles were performed with a ZetaSizer nano ZS (Malvern Instruments, Malvern, UK) at a temperature of 25 ± 0.1 °C. Samples were backscattered by a 4 mW He–Ne laser (operating at a wavelength of 633 nm) at an angle of 173°. At least 2 independent samples were taken, each of which was measured 3 up to 5 times.

Small-Angle X-ray Scattering (SAXS) Experiments: Small-angle X-ray scattering was recorded with a S3-MICRO SWAXS camera system (HECUS X-ray Systems, Graz, Austria). Cu Kα radiation of wavelength 1.542 Å was provided by a GeniX X-ray generator, operating at 50 kV and 1 mA. A 1D-PSD-50 M system (HECUS X-ray Systems, Graz, Austria) containing 1024 channels of width 54.0 μm was used for detection of scattered X-rays in the small-angle region. The working q-range ($Å^{-1}$) was $0.003 \leq q \leq 0.6$, where $q = 4\pi \sin(\theta)\lambda^{-1}$ is the modulus of the scattering wave vector. Thin-walled 2 mm glass capillaries were filled with the liposomal dispersions for the scattering experiments. The diffraction patterns were recorded for at least 3600 s. The solvent background scattering was subtracted from the intensity, and the resulting quantity was normalized and denoted as $I(q)$. The distance between the sample and detector was 265 mm. To minimize scattering from air, the camera volume was kept under vacuum during the measurements. Silver behenate (CH_3-$(CH_2)_{20}$-COOAg) with a d spacing value of 58.38 Å was used as a standard to calibrate the angular scale of the measured intensity. SAXS patterns were analyzed in terms of a global model using the program GAP (Global Analysis Program).[45–47] This technique models the full q-range in the SAXS regime including Bragg peaks and diffuse scattering. By this procedure, relevant structural parameters, as well as the distribution of electron density in the polar and apolar regions of membranes, were obtained. The GAP allows fitting the SAXS pattern of bilayer-based structures, that is vesicles and lamellar phases, using the following equation:

$$(q) = (1 - N_{diff})\frac{S(q)\left|F(q)\right|^2}{q^2} + N_{diff}\frac{\left|F(q)\right|^2}{q^2} \quad (1)$$

N_{diff} is the fraction number of positionally uncorrelated bilayers (i.e., those forming non-interacting vesicles) per scattering domain, $S(q)$ is the structure factor defining the spatial distribution of scatterers and describing the inter-particle interactions, while, $F(q)$ is the form factor given by the Fourier transform of the electron density. The electron density profile (ρ) can be modeled by the summation of 3 Gaussians distributions (as sketched in Scheme 1), two centered at the position of the electron-dense lipid head groups ($\pm z_H$) and a third, of negative amplitude, in the middle of the bilayer, where the hydrocarbon chains meet. The corresponding standard variation width of the Gaussians are given by σ_H and σ_C, respectively.[48,49]

The SAXS profile of unilamellar vesicles shows the typical diffuse scattering pattern of single, non-interacting bilayers and can be fitted by the form factor of locally flat objects. The global model does not require the presence of Bragg peaks at all, but may apply the same formalism to uncorrelated bilayers or unilamellar vesicles by just setting $N_{diff} = 1$ in Equation 1, that becomes:

$$I(q) = \frac{\left|F(q)\right|^2}{q^2} \quad (2)$$

From the SAXS analysis the membrane thickness (d_B) was obtained by using the formula $d_B = 2(z_H + 2\sigma_H)$, where z_H was derived from SAXS curve fitting with GAP.[49]

Cell Cultures and Treatments: Mouse 3T3 fibroblasts (ATCC collection) were grown at 37 °C in phenol red-free Dulbecco's modified Eagle's medium (DMEM, Invitrogen, USA) with high glucose, supplemented with 10% (v/v) fetal bovine serum, penicillin (100 U mL^{-1}), and streptomycin (100 μg mL^{-1}) (Invitrogen) in 5% CO_2 incubator at 37 °C. Cells were grown in 35 mm dishes, and experiments were carried out two days after seeding, when cells had reached 80 - 90% confluence. Liposome formulations and LCh solutions were added to the cells at a concentration of 1:200 (10 μL of sample in 2 mL of medium), and incubated at 37 °C for 2, 4, 24, and 48 h. Oleic acid and monoolein were dissolved in DMSO at a concentration of 100 and 430 mM respectively. These concentrated solutions were added to the culture medium at a dilution 1:1000. For live cell imaging, after replacing the sample suspension with fresh serum-free medium, cells were loaded with fluorescent probes, that after incubation time were washed out before imaging session. Cells were supravitally stained with the following probes (ex, em = fluorescence excitation and emission): 300 nM Nile Red (9-diethylamino-5H-benzo[α]phenoxazine-5-one) for 15 min (ex 470 ± 20, em 535 ± 40 for neutral lipids; ex 546 ± 6, em 620 ± 60 for cytoplasmic membrane); 650 nM Hoechst 33258 for 15 min (ex 360 ± 20, em 460 ± 25). Vehicles were DMSO for Nile Red and water for Hoechst. Stock solutions were 1000-fold concentrated not to exceed the 0.1% concentration of vehicle in the medium. Nile Red was from Fluka (Buchs, SG, Switzerland), Hoechst from Sigma-Aldrich (St Louis, MO, USA). The Nile Red is an ideal probe for the detection of lipids, as it exhibits high affinity, specificity and sensitivity to the degree of hydrophobicity of lipids. The latter feature results in a shift in the fluorescence emission, from red to green, correlating with the level of hydrophobicity of lipids.[50] Accordingly, cytoplasmic membranes mostly composed of phospholipids are generally stained in red, whereas neutral lipids encased in the lipid droplets are stained in green. Hoechst is a blue dye used for counterstaining the nucleus and to evaluate cell proliferation or chromatin condensation.

Fluorescence Microscopy and Image Analysis: Light microscopy observations were made using a Zeiss (Axioskop) upright fluorescence microscope (Zeiss, Oberkochen, Germany) equipped with 20× and

40×/0.75 NA water immersion objectives and a HBO 50 W L-2 mercury lamp (Osram, Berlin, Germany). Twelve-bit-deep images were acquired with a monochrome cooled CCD camera (QICAM, Qimaging, Canada) with variable exposure. The adopted filters allowed a virtually complete separation of the emissions and the simultaneous observation of the Nile Red and Hoechst probes. In general, microscope operations (filter exchanges, exposure time settings and focus adjustments) required an interval of 30–60 s between images of different fluorochromes. This resulted in a slight displacement of structures, because of live cell movements. Image analysis and quantification of lipid droplets were performed with Image Pro Plus software (Media Cybernetics, Silver Springs, MD).

MTT Assay for Cell Viability: Cell viability was analyzed by the MTT (3(4,5-dimethylthiazolyl-2)-2, 5-diphenyltetrazolium bromide, Sigma) colorimetric assay. 3T3 fibroblasts were seeded in 24-well plates (3×10^4 cell/well) and cultured overnight in serum-containing media. Then cells were incubated in the presence of the different liposome formulations (1:200, 2.5 µL of liposome formulation in 500 µL of medium), monoolein (430 µM in DMSO) and LCh solutions (47, and 202 µM) for 2, 4, 24 and 48 h at 37 °C. MO and LCh solutions are equimolar with the lipid and surfactant present in the liposome formulations. Treated cells were incubated with MTT (0.5 mg mL^{-1}) for 2 h at 37 °C. Then, media were removed, and cells were lysed with DMSO. Absorbance was measured at 570 nm using a microplate reader (Synergy 4, Synergy Multi-Detection Microplate Reader, BioTek Instruments). All measurements were performed in triplicate and repeated at least three times. Results are shown as percent of cell viability in comparison with non-treated control cells.

Statistics: Statistical analysis was carried out with Excel (Microsoft Co., Redmond, WA). Results were expressed as a mean ± standard deviation (SD). Statistically significant difference was evaluated by two sample t test with $p < 0.001$ as a minimal level of significance.

Gel Preparation: Hydroxypropylmethyl cellulose (HPMC) gel (2%) was prepared by carefully hydrating and slowly stirring the polymer at room temperature for 24 h to ensure uniform mixing while avoiding bubble production. After gel formation acid diclofenac was incorporated, at the same concentration of the liposomal formulation, under constant stirring.

Drug Loading Efficiency (E%): Liposome dispersions loaded with DCFH (LDH) were separated from the unentrapped material by gel chromatography on Sephadex G75. Sephadex was allowed to swell in water for two hours, and than in a 50-cm column fitted with the polymer dispersion. 1 mL of formulation was loaded on Sephadex, and than eluated samples were assayed for drug content. Drug loading efficiency, expressed as the percentage of the amount of drug initially used, was determined by high performance liquid chromatography (HPLC) after disruption of vesicles with 0.025% non-ionic Triton X-100. Diclofenac content was quantified at 227 nm using a chromatograph Alliance 2690 (Waters, Italy). The column was a Symmetry C18 (3.5 µ, 4.6 × 100 mm, Waters). The mobile phase was a mixture of 30% water and 70% acetonitrile (v/v), delivered at a flow rate of 0.5 mL min^{-1}. A standard calibration curve (peak area of diclofenac versus known drug concentration) was built up by using working, standard solutions (1.0–0.01 mg/mL). Calibration graphs were plotted according to the linear regression analysis, which gave a correlation coefficient value (R2) of 0.998. The DCFH retention time was 1.5 minutes, and the minimum detectable amount was 2 ng/mL.

Deformability Measurements: Liposome dispersion was extruded at constant pressure through 19-mm polycarbonate filters of definite pore size (50 nm), using an extrusion device Liposofast (Avestin, Canada).

Ex Vivo Skin Penetration and Permeation Studies: Experiments were performed non-occlusively by means of Franz diffusion vertical cells with an effective diffusion area of 0.785 cm^2, using newborn pig skin. One-day-old Goland–Pietrain hybrid pigs (about 1.2 kg) were provided by a local slaughterhouse. The skin, stored at –80 °C, was pre-equilibrated in physiological solution at 25 °C, two hours before the experiments. Skin specimens (n = 6 per formulation) were sandwiched securely between donor and receptor compartments of the Franz cells, with the *stratum corneum* (SC) side facing the donor compartment. The receptor compartment was filled with 5.5 mL of physiological solution, which was continuously stirred with a small magnetic bar, and thermostated at 37 ± 1 °C throughout the experiments to reach the physiological skin temperature (i.e., 32 ± 1 °C). 100 µL of the formulation to be tested (0.1% DCFH loaded liposome or gel formulation) was placed onto the skin surface (6 cells for each formulation). At regular intervals of 2 h, up to 24 h, the receiving solution was withdrawn and analyzed by HPLC for drug content. After 24 h, the skin surface of specimens was washed and the SC was removed by stripping with adhesive tape Tesa AG (Hamburg, Germany). Each piece of the adhesive tape was firmly pressed on the skin surface and rapidly pulled off with one fluent stroke. The epidermis was separated from the dermis with a surgical sterile scalpel. Tape strips, epidermis, and dermis were placed each in methanol, sonicated to extract the drug and then assayed for drug content by HPLC.

Acknowledgements

MIUR (PRIN 2008, grant number 2006030935) is acknowledge for financial support. The Scientific Park 'Sardegna Ricerche' (Pula, CA, Italy) is acknowledged for free access to SAXS.

Received: August 22, 2012
Published online: November 2, 2012

[1] M. Malmsten, *Soft Matter* **2006**, *2*, 760.
[2] E. Soussan, S. Cassel, M. Blanzat, I. Rico-Lattes, *Angew. Chem. Int. Ed.* **2009**, *48*, 274.
[3] P. Hiwale, S. Lampis, G. Conti, C. Caddeo, S. Murgia, A. M. Fadda, M. Monduzzi, *Biomacromolecules* **2011**, *12*, 3186.
[4] L. Zha, B. Banik, F. Alexis, *Soft Matter* **2011**, *7*, 5908.
[5] F. Cuomo, F. Lopez, A. Ceglie, L. Maiuro, M. G. Miguel, B. Lindman, *Soft Matter* **2012**, *8*, 4415.
[6] M. Liong, J. Lu, M. Kovochich, T. Xia, S. G. Ruehm, A. E. Nel, F. Tamanoi, J. I. Zink, *ACS Nano* **2008**, *2*, 889.
[7] C. Sun, J. S. H. Lee, M. Zhang, *Adv. Drug Deliv. Rev.* **2008**, *60*, 1252.
[8] M. S. Bhattacharyya, P. Hiwale, M. Piras, L. Medda, D. Steri, M. Piludu, A. Salis, M. Monduzzi, *J. Phys. Chem. C* **2010**, *114*, 19928.
[9] R. Angius, S. Murgia, D. Berti, P. Baglioni, M. Monduzzi, *J. Phys.: Condens. Matter* **2006**, *18*, S2203.
[10] F. Caboi, S. Murgia, M. Monduzzi, P. Lazzari, *Langmuir* **2002**, *18*, 7916.
[11] S. Mele, S. Murgia, F. Caboi, M. Monduzzi, *Langmuir* **2004**, *20*, 5241.
[12] S. Murgia, F. Caboi, M. Monduzzi, *Chem. Phys. Lipids* **2001**, *110*, 11.
[13] S. Murgia, S. Lampis, R. Angius, D. Berti, M. Monduzzi, *J. Phys. Chem. B* **2009**, *113*, 9205.
[14] J. Shah, Y. Sadhale, D. M. Chilukuri, *Adv. Drug Deliv. Rev.* **2001**, *47*, 229.
[15] M. Manconi, R. Isola, A. M. Falchi, C. Sinico, A. M. Fadda, *Colloids Surf. B* **2007**, *57*, 143.
[16] S. Murgia, S. Lampis, P. Zucca, E. Sanjust, M. Monduzzi, *J. Am. Chem. Soc.* **2010**, *132*, 16176.
[17] C. Peetla, A. Stine, V. Labhasetwar, *Mol. Pharm.* **2009**, *6*, 1264.
[18] M. Mezei, V. Gulasekharam, *Life Sci.* **1980**, *26*, 1473.
[19] M. M. A. Elsayed, O. Y. Abdallah, V. F. Naggar, N. M. Khalafallah, *Int. J. Pharm.* **2007**, *332*, 1.
[20] M. L. Gonzalez-Rodriguez, A. M. Rabasco, *Expert Opin. Drug Deliv.* **2011**, *8*, 857.
[21] G. Cevc, G. Blume, *Biochim. Biophys. Acta* **1992**, *1104*, 226.
[22] G. Cevc, A. Shatzlein, H. Richardsen, *Biochim. Biophys. Acta* **2002**, *1564*, 21.

[23] E. Touitou, M. Alkabes, N. Dayan, *Pharm. Res.* **1997**, *S14*, 305.
[24] E. Touitou, N. Dayan, L. Bergelson, B. Godin, M. Eliaz, *J. Controlled Release* **2000**, *65*, 403.
[25] M. J. Choi, H. I. Maibach, *Skin Pharmacol. Physiol.* **2005**, *18*, 209.
[26] A. Manosroi, P. Khanrin, W. Lohcharoenkal, R. G. Werner, F. Gotz, W. Manosroi, J. Manosroi, *Int. J. Pharm.* **2010**, *392*, 304.
[27] G. M. El Maghraby, B. W. Barry, A. C. Williams, *Eur. J. Pharm. Sci.* **2008**, *34*, 203.
[28] B. Geusens, M. V. Gele, S. Braat, S. C. D. Smedt, M. C. A. Stuart, T. W. Prow, W. Sanchez, M. S. Roberts, N. N. Sanders, J. Lambert, *Adv. Funct. Mater.* **2010**, *20*, 4077.
[29] C. Sinico, A. M. Fadda, *Expert Opin. Drug Deliv.* **2009**, *6*, 813.
[30] R. H. H. Neubert, *Eur. J. Pharm. Biopharm.* **2011**, *77*, 1.
[31] Y.-K. Song, C.-K. Kim, *Biomaterials* **2006**, *27*, 271.
[32] S. Murgia, A. M. Falchi, M. Mano, S. Lampis, R. Angius, A. M. Carnerup, J. Schmidt, G. Diaz, M. Giacca, Y. Talmon, M. Monduzzi, *J. Phys. Chem. B* **2010**, *114*, 3518.
[33] T. Loftsson, G. Somogyi, N. Bodor, *Acta Pharm. Nord.* **1989**, *1*, 279.
[34] L. B. Lopes, J. H. Collett, M. V. L. B. Bentley, *Eur. J. Pharm. Biopharm.* **2005**, *60*, 25.
[35] D. P. Siegel, J. L. Burns, M. H. Chestnut, Y. Talmon, *Biophys. J.* **1989**, *56*, 161.
[36] D. D. Lasic, R. Joannic, B. C. Keller, P. M. Frederik, L. Auvray, *Adv. Coll. Interf. Sci.* **2001**, *89-90*, 337.
[37] J. Briggs, H. Chung, M. Caffrey, *J. Phys. II* **1996**, *6*, 723.
[38] Y. Fujimoto, J. Onoduka, K. J. Homma, S. Yamaguchi, M. Mori, Y. Higashi, M. Makita, T. Kinoshita, J.-i. Noda, H. Itabe, T. Takanoa, *Biol. Pharm. Bull.* **2006**, *29*, 2174.
[39] T. N. Engelbrecht, A. Schroeter, T. Haub, R. H. H. Neubert, *Biochim. Biophys. Acta* **2011**, *1808*, 2798.
[40] C.-L. E. Yen, S. J. Stone, S. Koliwad, C. Harris, R. V. Farese, *J. Lipid Res.* **2008**, *49*, 2283.
[41] G. Diaz, B. Batetta, F. Sanna, S. Uda, C. Reali, F. Angius, M. Melis, A. Falchi, *Histochem. Cell Biol.* **2008**, *129*, 611.
[42] H. Ferreira, M. Lúcio, J. L. F. C. Lima, C. Matos, S. Reis, *Anal. Bioanal. Chem.* **2005**, *382*, 1256.
[43] P. Karande, S. Mitragotri, *Biochim. Biophys. Acta* **2009**, *1788*, 2362.
[44] P. Karande, A. Jain, K. Ergun, V. Kispersky, S. Mitragotri, *Proc. Natl. Acad. Sci. U.S.A.* **2005**, *102*, 4688.
[45] G. Pabst, *Biophys. Rev. Lett.* **2006**, *1*, 57.
[46] G. Pabst, R. Koschuch, B. Pozo-Navas, M. Rappolt, K. Lohner, P. Laggner, *J. Appl. Crystallogr.* **2003**, *63*, 1378.
[47] G. Pabst, M. Rappolt, H. Amenitsch, P. Laggner, *Phys. Rev. E* **2000**, *62*, 4000.
[48] L. Cantù, M. Corti, E. Del Favero, M. Dubois, T. N. Zemb, *J. Phys. Chem. B* **1998**, *102*, 5737.
[49] G. Pabst, J. Katsaras, V. A. Raghunathan, M. Rappolt, *Langmuir* **2003**, *19*, 1716.
[50] P. Greenspan, E. P. Mayer, S. D. Fowler, *J. Cell. Biol.* **1985**, *100*, 965.